CLIMATOLOGY

Abrupt Heinrich Stadial 1 cooling missing in Greenland oxygen isotopes

Chengfei He[1,2,3], Zhengyu Liu[2,4]*, Bette L. Otto-Bliesner[5], Esther C. Brady[5], Chenyu Zhu[3,6], Robert Tomas[5], Christo Buizert[7], Jeffrey P. Severinghaus[8]

Abrupt climate changes during the last deglaciation have been well preserved in proxy records across the globe. However, one long-standing puzzle is the apparent absence of the onset of the Heinrich Stadial 1 (HS1) cold event around 18 ka in Greenland ice core oxygen isotope $\delta^{18}O$ records, inconsistent with other proxies. Here, combining proxy records with an isotope-enabled transient deglacial simulation, we propose that a substantial HS1 cooling onset did indeed occur over the Arctic in winter. However, this cooling signal in the depleted oxygen isotopic composition is completely compensated by the enrichment because of the loss of winter precipitation in response to sea ice expansion associated with AMOC slowdown during extreme glacial climate. In contrast, the Arctic summer warmed during HS1 and YD because of increased insolation and greenhouse gases, consistent with snowline reconstructions. Our work suggests that Greenland $\delta^{18}O$ may substantially underestimate temperature variability during cold glacial conditions.

INTRODUCTION

Glacial periods exhibit Dansgaard-Oeschger (DO) and Heinrich modes of abrupt climate variability, both of which are linked to changes in Atlantic meridional overturning circulation (AMOC) (*1*, *2*). Heinrich stadials are generally believed to represent more-complete AMOC shutdown and, thus, more-extreme winter cooling than DO stadials (*3*). Greenland ice core $\delta^{18}O$ of water isotopes is a commonly used proxy for site temperature due to the "temperature effect" (*4*) and has been considered as a key index that records abrupt climate changes around the Arctic region. However, Greenland $\delta^{18}O$ fails to differentiate the DO and Heinrich stadials from similar $\delta^{18}O$ levels in Heinrich stadials and regular DO stadials. This contrasts proxies for Atlantic circulation and temperature (*5*, *6*) and Asian monsoon (*7*) that show clearly distinct signatures of the Heinrich stadials. Consequently, the commonly used Greenland event stratigraphy (*8*) only identifies DO stadial-interstadial transitions but not Heinrich stadials. These contrasting observations raise a fundamental question: Was Greenland climate not affected by Heinrich variability, or was Heinrich variability not recorded in Greenland $\delta^{18}O$?

Northern Hemisphere climate during the last deglaciation was punctuated by abrupt events such as Heinrich Stadial 1 [HS1; ~18 to 14.7 thousand years ago (ka)], Bølling-Allerød warming (BA; 14.7 to 12.9 ka), and Younger Dryas cooling (YD; 12.9 to 11.7 ka). These events occur coherently in Northern Hemisphere proxy records (Fig. 1) (*9*, *10*). Here, we focus on the last Heinrich event, the HS1, a period of weakened AMOC from 18 to 14.7 ka before present (BP) (*11*), which contains the abrupt Heinrich event 1 ice-rafted debris layers around 16.2 ka BP (*12*), while Greenland $\delta^{18}O$ shows virtually no depletion signal around the HS1 onset at ~18 ka BP (Fig. 1B and fig. S1) (*13*, *14*). This is in contrast to other proxies across the Northern Hemisphere (Fig. 1, E and F) (*9*, *10*), from North Atlantic sea surface temperature (SST) (Fig. 1E) (*15*) to Asian monsoon speleothem calcite isotope $\delta^{18}O_c$ (Fig. 1F) (*7*). This apparent lack of $\delta^{18}O$ response over Greenland has led to the speculation that Greenland did not cool during HS1, implying a decoupling of the Arctic from hemispheric climate trends (*16*). Here, combining climate proxies with transient isotope-enabled climate model simulations, we resolve this puzzle and suggest that the HS1 cooling did occur but was not recorded in ice core $\delta^{18}O$.

RESULTS

Deglacial evolution of water isotopes and climate

We simulate the coevolution of climate and water isotopes during the last deglaciation (20 to 11 ka) in the water isotope–enabled Community Earth System Model (iCESM) (*17*). We perform a set of four simulations with four realistic forcing factors (Fig. 1A) applied additively: first, ice sheet and bathymetry (ICE), then insolation (ICE+ORB), the greenhouse gases (ICE+ORB+GHG), and, last, meltwater fluxes (ICE+ORB+GHG+MWF) or iTRACE, for the isotope-enabled transient climate experiment (*18*).

iTRACE quantitatively captures many major features of water isotopes and climate variations during the last deglaciation from the North Atlantic SST to Asian monsoon $\delta^{18}O_c$ (Fig. 1, E and F). Overall, global surface temperature rises during the deglaciation, with an interhemispheric bipolar seesaw during HS1 and YD in response to the AMOC slowdown that is forced by meltwater fluxes mainly to the North Atlantic (Fig. 1, A and G). Over Greenland, the model simulates clear BA and YD events that match reconstructed changes in precipitation $\delta^{18}O$ (~4‰), temperature (~11°C), and the variation of snowfall accumulation rate (Fig. 1, B to D). The corresponding overall temporal $\Delta\delta^{18}O/\Delta T$ regression slope from 20 to 11 ka is ~0.36‰ K^{-1} [as can also be estimated directly from Fig. 1 (B and C) as ≈4‰/11°C], broadly consistent with reconstructions from borehole temperature (*19*), deuterium excess (*20*), nitrogen and argon isotope fractionation (*21*), and a reanalysis technique (Fig. 1C) (*22*). Simulated mean annual $\delta^{18}O$ remains stable through HS1 from central

[1]College of Atmospheric Sciences, Nanjing University of Information Science and Technology, Nanjing, China. [2]Department of Geography, The Ohio State University, Columbus, OH 43210, USA. [3]Open Studio for Ocean-Climate-Isotope Modeling, Pilot National Laboratory for Marine Science and Technology, Qingdao, China. [4]College of Geography Sciences, Nanjing Normal University, Nanjing, China. [5]Climate and Global Dynamics Laboratory, National Center for Atmospheric Research, Boulder, CO 80305, USA. [6]Key Laboratory of Physical Oceanography, Ocean University of China, Qingdao, China. [7]College of Earth, Ocean, and Atmospheric Sciences, Oregon State University, Corvallis, OR 97331, USA. [8]Scripps Institution of Oceanography, University of California, San Diego, La Jolla, CA 92037, USA.
*Corresponding author. Email: liu.7022@osu.edu

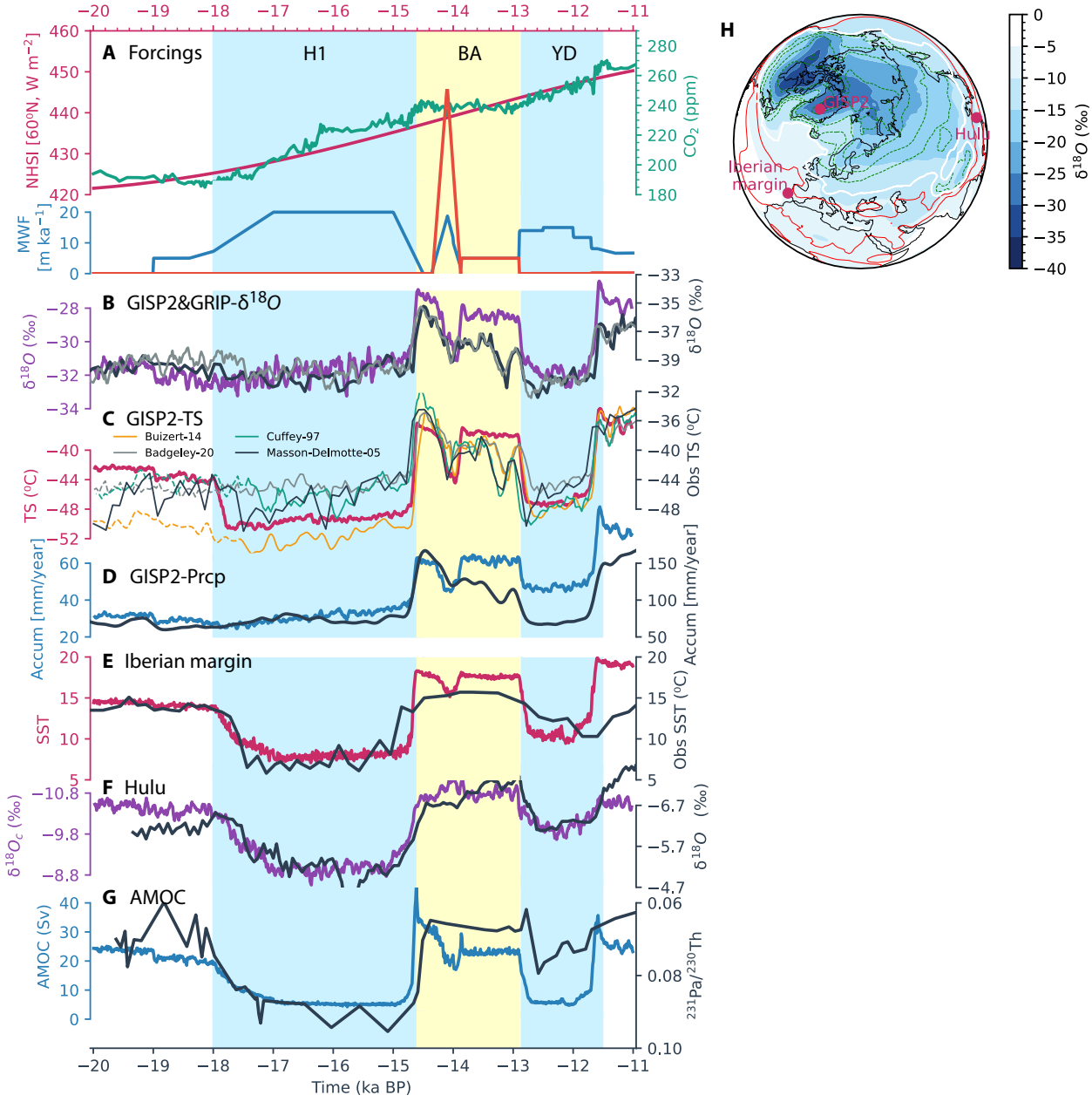

Fig. 1. Water isotope–climate evolution during the last deglaciation. (**A**) Climate forcings including June solar insolation at 60°N (red), CO_2 concentration (green), meltwater forcing at the Northern Hemisphere (blue) and the Southern Hemisphere (orange). ppm, parts per million. (**B**) Modeled (purple) and observed ice core $\delta^{18}O$ at Greenland Ice Sheet Project 2 (GISP2) (black) (*13*) and GRIP (gray) (*49*). (**C**) As in (B) but for modeled (red) and reconstructed (see legends and text) temperature. (**D**) As in (B) but for modeled (blue) and reconstructed (black) (*28*) ice accumulation rate. (**E**) Modeled (red) and observed (black) SST at the Iberian margin. (**F**) Modeled (purple) and observed (black) (*7*) speleothem $\delta^{18}O_c$ in Hulu Cave. (**G**) Modeled AMOC intensity (blue) and $^{231}Pa/^{230}Th$ in sediment core GGC5 as a proxy for AMOC intensity (black) (*11*). (**H**) Model global distribution of $\delta^{18}O$ and temperature at Last Glacial Maximum (LGM). In (B, C, E, and F), the scales are the same in the model and observation but with an offset. In (D), the scale of reconstructed ice accumulation rate is 2.5 times larger than the modeled one. In (F), the modeled speleothem $\delta^{18}O_c$ is calculated as $\delta^{18}O_c = \delta^{18}O - 0.24\Delta T$, with ΔT as the annual temperature anomaly from LGM (*18*). In (H), red (green) contours represent temperature above (below) zero (counter interval, 5°C), with the white contour as 0°C. A five-decade running mean is applied to model time series.

to northern Greenland (fig. S2), consistent with ice core records there (Fig. 1B and fig. S1, A and B). This muted $\delta^{18}O$ response in Greenland summit, however, is accompanied by an abrupt cooling in model mean annual temperature of ~6°C at the HS1 onset (~18 ka), more than half the magnitude of the abrupt changes in BA and YD (Fig. 1B and fig. S2).

On the basis of the analysis of our simulation and available climate proxies, we hypothesize that HS1 cooling did occur in the Arctic but the cooling signal is virtually absent in ice core $\delta^{18}O$. At face value, the simulated ~6°C HS1 mean annual cooling appears to contradict existing Greenland $\delta^{18}O$-based temperature reconstructions that do not show such cooling (Fig. 1C). However, most existing

reconstructions rely on $\delta^{18}O$ and use either borehole temperatures (*19*), nitrogen isotopic fractionation (*21*), or reanalysis techniques (*22*) to calibrate the $\delta^{18}O$-temperature slope. These $\delta^{18}O$-based methods are therefore incapable of detecting any abrupt cooling that is not accompanied by a $\delta^{18}O$ decrease. One reconstruction did find a ~3° to 4°C HS1 cooling via a method that combines $\delta^{18}O$ and deuterium excess (Fig. 1C) (*20*). This cooling is contributed partly by a small $\delta^{18}O$ decrease in the Greenland Ice Core Project (GRIP) ice core (Fig. 1B). However, this method still assumes a stable $\delta^{18}O$-temperature relationship over time and would consequently underestimate HS1 cooling in the case of a muted $\delta^{18}O$ response. Our muted $\delta^{18}O$ hypothesis, therefore, does not contradict any existing Greenland deglacial ice core temperature reconstructions.

Furthermore, an HS1 cooling in the Arctic is consistent with the global climatic fingerprint in response to AMOC slowdown. Climate models show consistently a characteristic global climate fingerprint response to AMOC slowdown that includes Arctic and circum–North Atlantic cooling, a southward shift of the Intertropical Convergence Zone and weakening of Northern Hemisphere monsoons, and a warming in the Southern Hemisphere due to the bipolar seesaw response (*23*–*26*). This fingerprint at the HS1 onset has been detected in many proxy records outside the Arctic (Fig. 1, E and F) (*9*, *10*). The absence of HS1 cooling in the Arctic would therefore imply a highly anomalous deviation from the expected global climatic fingerprint. Last, mean annual ice core $\delta^{18}O$ does broadly follow mean annual temperature closely after HS1. This suggests that Greenland $\delta^{18}O$ may not be a uniformly valid proxy for temperature across the deglaciation, in particular, during periods of extreme cold.

Suppression of $\delta^{18}O$ variability

It has been suggested that the Greenland $\delta^{18}O$-temperature slope $\Delta\delta^{18}O/\Delta T$ can be reduced by increased precipitation seasonality that is caused by winter cooling and drying associated with North Atlantic sea ice expansion (*14*, *19*, *27*–*32*) in response to AMOC slowdown (*33*, *34*). Our simulations imply that the temporal slope was reduced even further to around ~0‰ K^{-1} at the HS1 onset. The key question here is why is the $\delta^{18}O$ muted at the HS1 onset but not during later stages of the deglaciation in BA and YD? This requires a quantitative assessment of all the effects on Greenland $\delta^{18}O$.

We decompose the ice core $\delta^{18}O$ change approximately into the changes in annual isotopic composition $\Delta\delta^{18}O_{ann}$ and precipitation seasonality ΔP_S as $\Delta\delta^{18}O \approx \Delta\delta^{18}O_{ann} + \Delta P_S$ (Materials and Methods and Fig. 2A) (*34*). The change of isotopic composition $\Delta\delta^{18}O_{ann}$ generally follows site temperature (Fig. 1C) via the temperature

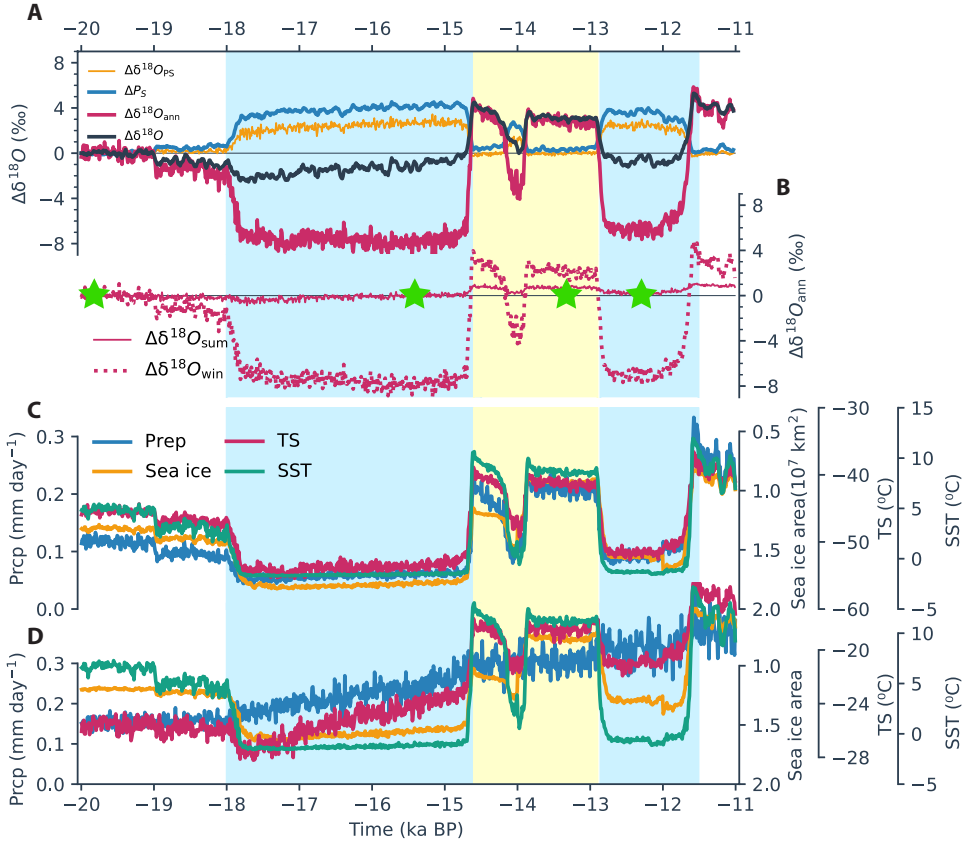

Fig. 2. Decomposition of ice core $\delta^{18}O$ at Greenland (70° to 80°N, 50° to 30°W). (**A**) Response of ice core $\delta^{18}O$ (black, $\Delta\delta^{18}O$), decomposed into the terms from the precipitation seasonality effect (blue, ΔP_S), annual mean of the isotopic composition (red, $\Delta\delta^{18}O_{ann}$), and residual seasonality (yellow, $\Delta\delta^{18}O_{PS}$; see Materials and Methods for the detailed definitions). (**B**) $\Delta\delta^{18}O_{ann}$ is further decomposed into summer [June, July, and August (JJA), solid] and winter (non-JJA, dotted) contributions. (**C**) Time series of total winter (September to May) precipitation (blue), surface air temperature (TS) (red) at Greenland, sea ice coverage (yellow), and SST over deep convection regions (green). (**D**) Same as (C) but for summer (JJA). In (B), the green stars correspond to the times of the moisture tagging experiments at LGM (20 ka), HS1 (15.5 ka), BA(13.2 ka), and YD(12.2 ka). In (C and D), deep convection is defined in the domain of 55° to 60°N, 40° to 20°W, where sea ice grows most in HS1 and YD, as shown in Fig. 3C.

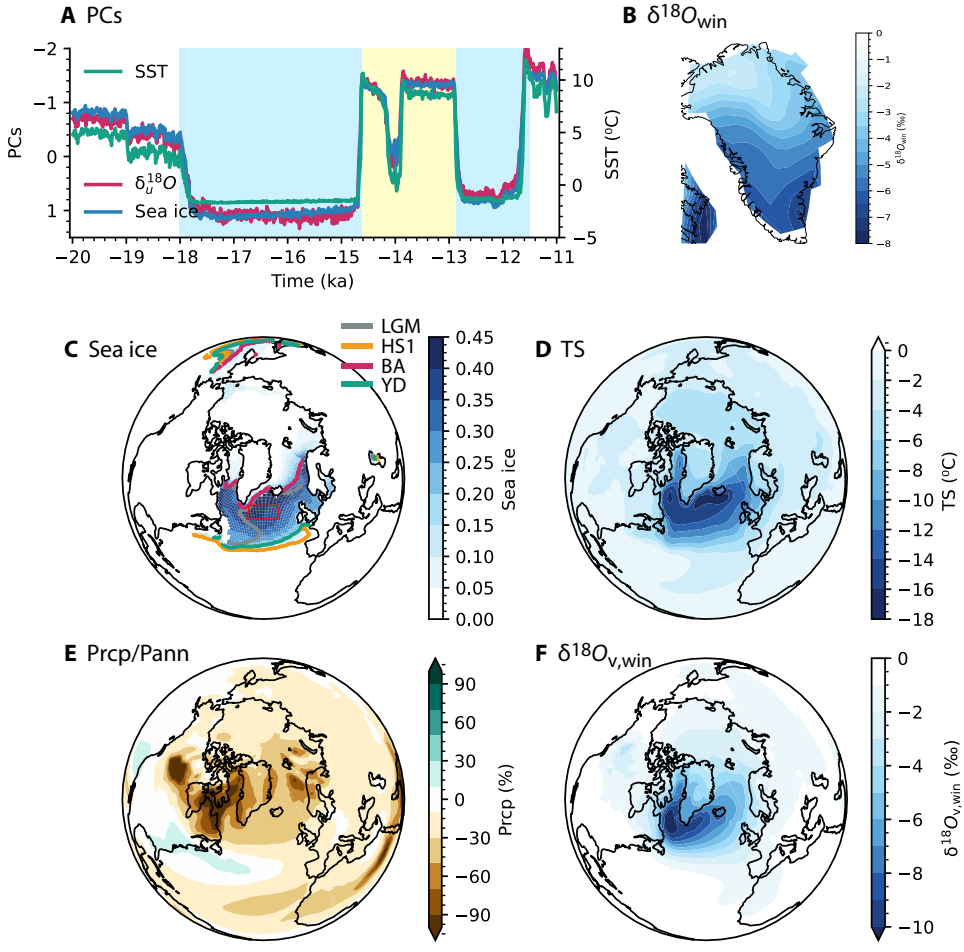

Fig. 3. Water isotope–climate–sea ice coherence in winter derived as first mode of MCA between $\delta^{18}O_{win}$ and sea ice fraction. (**A**) Normalized time expansion coefficients of the first MCA mode for $\delta^{18}O_{win}$ (red), sea ice (blue), and winter SST in the deep convection region [red box in (C)]. (**B**) $\delta^{18}O_{win}$ over Greenland regressed on the normalized time expansion coefficient of sea ice. (**C** to **F**) As in (B), but for sea ice fraction, surface air temperature, precipitation change percentage (Prcp) normalized by LGM climatology, and winter column weighted water vapor $\delta^{18}O_{v,win}$. Regression fields at 99% ($P < 0.01$) confidence level in two-tailed Student's *t* test are plotted. In (C), the curves correspond to sea ice margin defined as the 15% sea ice fraction in the ocean at different periods (see legend). In (F), the column water vapor $\delta^{18}O_{v,win}$ is weighted by the moisture in each layer. Prcp, Precipitation.

effect with a large temporal slope of $\Delta\delta^{18}O_{ann}/\Delta T \sim 1‰\ K^{-1}$, characterized by an abrupt isotopic depletion at the HS1 onset and clear BA/YD events. However, precipitation seasonality ΔP_S compensates the $\Delta\delta^{18}O_{ann}$ change such that the total $\Delta\delta^{18}O$ variability is suppressed relative to $\Delta\delta^{18}O_{ann}$ over Greenland (Fig. 2A). Qualitatively, this suppression is consistent with previous modeling studies for glacial climate changes (*31*) and for millennium-scale events in response to the AMOC (*33*, *34*), where it manifests as a low apparent isotope slope of $\Delta\delta^{18}O/\Delta T$ around ~0.4‰ K^{-1} (*21*, *35*). Quantitatively, however, our simulation suggests that for the Last Glacial Maximum (LGM) to HS1 transition, this compensation is almost complete, leading to negligible $\Delta\delta^{18}O$ at the HS1 onset (Fig. 2A) or an apparent slope close to 0‰ K^{-1} in central and northern Greenland (Fig. 1B and figs. S1 and S2), as well as, more generally, over much of the Arctic (fig. S3 and Supplementary Text). The difference in $\delta^{18}O$ responses between the onsets of HS1 and YD appears to be associated with different cooling magnitudes and then different extents of $\delta^{18}O_{ann} - \Delta P_S$ compensation in the two climate stages: The cooling and $\delta^{18}O_{ann}$ depletion in HS1 are about half of those in YD (−6‰ versus −12‰ and −5°C versus −10°C in the summit region) (Fig. 2A and fig. S4, A to D), while the ΔP_S enrichment is comparable in HS1 and YD (~+4‰) (with an additional +2‰ enrichment from a residual seasonality effect $\Delta\delta^{18}O_{PS}$; see Materials and Methods) (Fig. 2A). This leads to the $\delta^{18}O$ signal vanishing at HS1 but still being depleted at YD with half the $\delta^{18}O_{ann}$ depletion. While the model correctly simulates $\delta^{18}O$ at the HS1 onset in central and northern Greenland, the model is less successful in south and east Greenland where it simulates a greater $\delta^{18}O$ depletion than what is seen in the data, reflecting the model deficiency, which is partly caused by the lower altitude and the inability to resolve local topography in the model relative to the observation (fig. S1 and Supplementary Text).

Winter climate impact on $\Delta\delta^{18}O_{ann}$–ΔP_S compensation

The $\delta^{18}O$ signal is suppressed by the enhanced precipitation seasonality ΔP_S associated with extended precipitation from winter (broadly defined here as September to May) to summer (June, July, and August) during the cooling events HS1 and YD. For the abrupt onsets of HS1 and YD, the shifts of precipitation weight are mainly caused by

the abrupt loss of snowfall in winter (Fig. 2C and fig. S4, B and C), in response to the AMOC collapses that are here forced by meltwater discharge (fig. S5, A, C, and E). The winter drying increases the relative weight of summer precipitation abruptly (fig. S4C) in the mean annual signal in ice cores, incorporating more of the enriched summer oxygen isotopes (fig. S4D); the resulting ΔP_S enrichment opposes the $\Delta\delta^{18}O_{ann}$ depletion and suppresses $\delta^{18}O$ variability relative to $\delta^{18}O_{ann}$ (*31*, *33*, *34*).

The changes of winter climate and isotope composition $\Delta\delta^{18}O_{win}$ are further related to SST and sea ice cover over the subpolar North Atlantic (Fig. 2C and fig. S4, E and F), suggesting a role of sea ice in modulating the response of Greenland $\Delta\delta^{18}O$. The coherent variability between winter $\Delta\delta^{18}O_{win}$ and sea ice, notably the feature of a weaker change in HS1 onset than in YD, is well represented in the leading mode of maximum covariance analysis (MCA; explaining 99% covariance) (Fig. 3, A to C). Accompanying the southward expansion of sea ice is a strong $\Delta\delta^{18}O_{win}$ depletion and cooling, a decreased snowfall over Greenland and the Arctic, and a southward shift of the storm track that is indicated in the dipole response of precipitation (Fig. 3, B to E); the largest changes are seen surrounding southern Greenland in the subpolar North Atlantic, coinciding with the region of greatest sea ice change (Fig. 3, B to E). This coherent evolution of sea ice, $\Delta\delta^{18}O_{win}$, and winter climate is consistent with the mechanism of sea ice modulation of $\delta^{18}O$ variability via its impact on $\Delta\delta^{18}O_{ann} - \Delta P_S$ compensation (*32*, *34*), which is further confirmed in moisture tagging experiments (Materials and Methods, figs. S6 to S8, and Supplementary Text). In HS1 or YD, the collapsed AMOC reduces northward ocean heat transport, leading to SST cooling and sea ice expansion in the subpolar North Atlantic (Fig. 3A and fig. S4, E and F). This sea ice expansion cools the atmosphere by shutting off oceanic heat flux and increases the distance of moisture import from south of the sea ice margin over the North Atlantic, both effects favoring a depletion in atmospheric (vapor) $\delta^{18}O_v$ (Fig. 3F) and then in precipitation $\delta^{18}O_{win}$ over Greenland (Fig. 3B, fig. S7, and Supplementary Text). Meanwhile, the winter sea ice expansion reduces precipitation over Greenland by shielding the major winter moisture source from the North Atlantic (fig. S6 and Supplementary Text), leading to the reduction of winter snowfall (fig. S4, F to B) and ΔP_S enrichment (Fig. 2A and fig. S4C).

Sea ice extent at LGM mutes $\Delta\delta^{18}O$ at the HS1 onset

The extent of sea ice varies with the background climate. The LGM is much colder than the BA, leaving the winter SST over much of the subpolar North Atlantic close to the freezing point (–2°C). This leads to the SST cooling and then sea ice expansion from LGM to HS1 being only about half that from BA to YD (Figs. 2C and 3C) despite the fact that both transitions have a comparable reduction in AMOC strength. This then leads to the magnitude of the LGM-HS1 transition being about half as large as that of the BA-YD transition in many aspects, including the depletion in $\Delta\delta^{18}O_v$ ($\delta^{18}O$ in vapor) that is mainly from the Atlantic source (fig. S7 and Supplementary Text), precipitation $\Delta\delta^{18}O_{win}$, and $\Delta\delta^{18}O_{ann}$ (Fig. 2B). In particular, the reduction of moisture source from LGM to HS1 (0.13 to 0.07 ≈ 0.06 mm/day) is half that from BA to YD (0.21 to 0.09 ≈ 0.12 mm/day), mainly from the Atlantic source (fig. S6, E and F, and Supplementary Text). However, the total moisture source of the background climate at LGM (0.13 mm/day) is also half that at BA (0.21 mm/day) due to the larger sea ice cover at LGM, leading to the precipitation about half at LGM relative to BA in the model; this halved precipitation at the LGM relative to the BA is consistent with the observed accumulation rate (Fig. 1D). Together, the reduction of moisture source is ~50% for both the LGM-HS1 transition (0.06/0.13) and BA-YD transition (0.13/0.21) mainly from the Atlantic. This leads to a comparable (50%) reduction in winter precipitation weight (Fig. 2C and fig. S3, B and C) and then a comparable enrichment in ΔP_S (Fig. 2A) for both transitions. This enrichment effect due to the change of precipitation seasonality, mainly from ΔP_S, compensates the $\Delta\delta^{18}O_{ann}$ depletion completely at the onset of HS1, leading to the absence of ice core $\Delta\delta^{18}O$; in contrast, this ΔP_S enrichment only compensates half the $\Delta\delta^{18}O_{ann}$ depletion during YD, leaving another half as a depletion signal in the ice core $\Delta\delta^{18}O$.

The distinct impact of sea ice on Arctic climate for the LGM-HS1 transition is also shown in the distinctly abrupt cooling at ~18 ka. In contrast to the gradual meltwater discharge and the resulting gradual slowdown of AMOC and climate evolution in the mid-latitude and tropics that took over 1000 years (Fig. 1, A, E to G), the model cooling in the Arctic occurs abruptly in ~200 years at ~18 ka (Fig. 1C and fig. S2) because of the strongly nonlinear response of sea ice to climate forcing. In comparison, the abrupt changes associated with YD and BA are accompanied by abrupt changes of AMOC in ~100 years in response to either abrupt meltwater fluxes (at ~12.8 ka) or gradual meltwater fluxes (at ~14.6 and 11.6 ka) (Fig. 1), likely reflecting more the nonlinear response of the AMOC to meltwater forcing. Note that this abrupt cooling is not produced in the earlier study in TRACE-21 (*23*), which used an earlier model [Community Climate System Model version 3 (CCSM3)] of coarser resolution. The difference in temperature responses appears to be caused by a very weak sea ice sensitivity in CCSM3.

Summer warming during HS1 and YD

In contrast to the fluctuating temperature in winter and annual mean, model Arctic summer temperature increases almost linearly during the deglaciation (Fig. 2D). This summer warming appears to be decoupled from summer sea ice and SST over the North Atlantic (Fig. 2D and fig. S4) and represents an amplified continental response to increased summer insolation and GHG (fig. S5, B, D, and F). This simulated summer warming sheds light on another puzzle of the deglacial climate evolution, namely, the continued snowline retreat in Northern Europe and Greenland during the YD, despite this period being conventionally thought of as a cold period (*14*, *36*, *37*). The summer warming forces glacial retreat during the critical summer melt season, while the mean annual cooling occurred predominantly in winter and, therefore, had little impact on snowline. While this hypothesis has been proposed previously (*14*, *36*, *37*), a quantitative confirmation has remained challenging because of the potentially opposite temperature responses to different forcing factors, notably insolation, GHG, ICE, and meltwater, in addition to feedbacks within the climate system. Our simulations provide, to our knowledge, the first firm quantitative basis supporting this idea.

The summer warming is also important for the evolution of ice core $\delta^{18}O$ during HS1 and YD. Although winter climate is responsible for the abrupt signal in ice core $\delta^{18}O$, the summer warming, the associated northward shift of storm track and increased summer snowfall, also contributes substantially to an increasing trend of summer precipitation weight (Fig. 2D and fig. S4, B and C). This increasing trend of summer precipitation weight and the resulting ΔP_S enrichment allow the summer precipitation weight to remain elevated such that the ice core $\delta^{18}O$ remains absent and suppressed

during the entire periods of HS1 and YD, respectively. Our calculation shows that, without this summer wetting trend, summer precipitation weight would have decreased steadily in these two periods by a total of ~20%, reducing half of the weight increase caused by the abrupt winter drying and leading to a larger $\delta^{18}O$ signal in ice cores.

DISCUSSION

Our study suggests that a strong winter Arctic cooling occurred concurrent with hemispheric climate changes at the onset of HS1 in response to AMOC slowdown and the resulting sea ice expansion. This cooling signal, however, is virtually absent in Greenland ice core $\delta^{18}O$. The near absence of an ice core $\Delta\delta^{18}O$ signal at the HS1 onset suggests a strong dependence of the $\Delta\delta^{18}O/\Delta T$ sensitivity on background climate. In particular, during extreme cold winter climate of glacial period, the limited potential for further sea ice expansion mutes the ice core $\delta^{18}O$ response substantially via its impact on the precipitation seasonality ΔP_S and its compensation on isotopic composition $\Delta\delta^{18}O_{ann}$. Greenland ice core $\delta^{18}O$ variability and its paleothermometer scaling depend on the background climate as well as the magnitude of the event (*34*) and is therefore unlikely to have a uniform sensitivity to temperature during the deglaciation, as noted by previous studies of observations (*14*, *38*) and models (*31*–*33*, *39*). Despite the $\delta^{18}O$ compensation, the ice core $\Delta\delta^{18}O$ signal is dominated by the large fluctuating winter temperature signal and almost completely misses the summer temperature signal of an almost linear warming trend throughout the deglaciation.

Our study further implies that Arctic climate underwent even greater abrupt changes than those inferred from the Greenland ice core $\delta^{18}O$, not only for HS1 but also for other Heinrich stadials during the glacial periods in general. Under the glacial conditions, the large background sea ice leads to a strong $\delta^{18}O$ compensating effect such that the depletion in the ice core $\delta^{18}O$ tend to be limited by a lower bound despite strong cooling.

MATERIALS AND METHODS

The iTRACE simulation

The iTRACE is performed in the state-of-the-art iCESM1.3 but with water isotopes enabled (*18*), largely following the strategy of the previous transient simulation TRACE-21 (*23*). The incorporation of water isotope enables us to compare the modeled water isotopes with the observation directly to better understand past climate changes. The iCESM1.3 (*17*) is composed of the community atmosphere model (CAM5.3), Parallel Ocean Program (version 2), Los Alamos Sea Ice Model (version 4), and Community Land Model (version 4). The resolution of atmosphere and land is nominal 2° resolutions (1.9° in latitude and 2.5° in longitude), with 30 vertical levels in the atmosphere; the resolution of ocean and sea ice is nominal 1° horizontal resolutions (gx1v6), with 60 vertical levels in the ocean. Our iCESM1.3 reproduces the present-day physical climate reasonably well, similar to CESM1.2 (*40*). The spatial distribution and seasonal cycle of water isotope are reproduced reasonably well over the Arctic and Asia (*17*). There are, nevertheless, some model biases. For example, the mean annual precipitation $\delta^{18}O$ at Greenland tends to be enriched compared with observations, partly, because model Greenland ice sheet (fig. S2A) is lower than that in the real world by ~300 to 400 m (fig. S1E).

The model LGM (20 ka) state was derived by a spin up for 1000 years from an earlier CCSM4 LGM simulation. This LGM simulation was spun up from 2250 years from a state in which the ocean state was initialized from the present-day observations, with a constant value of 1.05‰ added to $\delta^{18}O$ to account for the isotopically enriched seawater caused by the increased LGM ice sheet volume. Our LGM state shows a global mean temperature about 6° to 7°C cooler than the preindustrial, an AMOC of transport of about 25 Sv close to the model preindustrial, but with a shallower depth. Over the summit (70° to 80°N, 50 to 30°W), the mean annual precipitation (snow) accumulation at LGM is ~50 mm/year, comparable to the reconstructed observation (Fig. 1D and fig. S4B). The spatial slope over Greenland $\delta^{18}O$ is around 0.8‰/°C, consistent with the observation. The sea ice covers the Nordic Sea and the western subpolar North Atlantic (Fig. 3A), consistent with reconstructions (*41*, *42*). Starting from 20 ka, all experiments were integrated to 11 ka. First, three parallel experiments were branched off with three forcing factors added one by one: first, the ice sheet (ICE-6G), then the orbital forcing (*43*), and, last, the greenhouse gases (*44*), forming three transient sensitivity experiments, ICE, ICE+ORB, and ICE+ORB+GHG, respectively. The baseline iTRACE simulation (also ICE+ORB+GHG+MWF) is branched off from the ICE+ORB+GHG run at 19 ka, with the MWF imposed largely similar to that in TRACE-21ka (Fig. 1A). The $\delta^{18}O$ values in the meltwater were prescribed according to (*45*), and the δD values in the meltwater were the $\delta^{18}O$ values multiplied by a factor of 8. During the simulation, we change the ice sheet every thousand years (at 19 ka, 18 ka, 17 ka,…) and modified the ocean bathymetry twice at 14 and 12 ka on the basis of the ICE-6G reconstruction (*46*). These experiments allow us to estimate the impact of each forcing effect approximately as follows: ice sheet (ICE), orbital (ICE+ORB − ICE), greenhouse gases (ICE+ORB+GHG − ICE+ORB), and meltwater flux (iTRACE − ICE+ORB+GHG).

Global surface temperature in iTRACE rises with an interhemisphere bipolar seesaw during HS1 and YD, broadly consistent with reconstructions (*9*, *10*). Our preliminary analyses further show that iTRACE is in good agreement with reconstructions in precipitation $\delta^{18}O$ and climate over the entire pan-Asian monsoon region (*18*). We also note several improvements of the model climate of iTRACE simulation over TRACE-21 (*23*) because of the improved climate model, model resolution, and the incorporation of water isotopes. For the purpose of studying Greenland here, in comparison with reconstructions, the overall temperature evolution during the deglaciation is much improved in iTRACE (Fig. 1C) compared to TRACE-21, especially after the BA, because the latter failed in simulating the resumption of AMOC after the YD (*47*).

Decomposition of $\delta^{18}O$ response

The ice core water isotope is accumulated in precipitation and therefore can be calculated as the total precipitation weighted isotope

$$\delta^{18}O = \Sigma_{m=1}^{12} \delta^{18}O_m \frac{P_m}{P} \quad (1)$$

where $\delta^{18}O_m$ is the oxygen isotope composition of calendar month m in precipitation, P_m is the precipitation amount of month m, with the sum as the annual precipitation amount $P = \Sigma_{m=1}^{12} P_m$. The response of the ice core water isotope can thus be decomposed as in (*48*)

$$\Delta\delta^{18}O = \Delta P_s + \Delta\delta^{18}O_s \quad (2)$$

where

$$\Delta P_s = \sum_{m=1}^{12}\Delta\left(\frac{P_m}{P}\right)\delta^{18}O_m,\ \Delta\delta^{18}O_s = \sum_{m=1}^{12}\left(\frac{P_m}{P}\right)\Delta\delta^{18}O_m \quad (3)$$

Here, ΔP_s is caused by the change of the season cycle of precipitation or precipitation seasonality. Since $\sum_{m=1}^{12}\frac{P_m}{P} = 1$, the change of precipitation weight is constrained as $\sum_{m=1}^{12}\Delta\left(\frac{P_m}{P}\right) = 0$. As a result, this term can be rewritten as

$$\Delta P_s = \sum_{m=1}^{12}\Delta\left(\frac{P_m}{\mathbf{P}}\right)(\delta^{18}O_m - \delta^{18}O_{ann}) \quad (4)$$

where

$$\delta^{18}O_{ann} = \sum_{m=1}^{12}\frac{\delta^{18}O_m}{12} \quad (5)$$

is the (arithmetic) mean annual of the isotopic composition. Normally, warm (cold) season has higher (lower) $\delta^{18}O_m$, and therefore, $\delta^{18}O_m - \delta^{18}O_{ann} > 0$ (<0). Therefore, if the seasonal cycle of rainfall shifts from winter to summer, as in the case of HS1 and YD (fig. S4C), $\Delta P_s > 0$ is enrichment (Fig. 2A).

The term $\Delta\delta^{18}O_s$ can be further decomposed as

$$\Delta\delta^{18}O_s = \Delta\delta^{18}O_{ann} + \Delta\delta^{18}O_{PS} \quad (6)$$

where

$$\Delta\delta^{18}O_{ann} = \sum_{m=1}^{12}\frac{\Delta\delta^{18}O_m}{12},\ \Delta\delta^{18}O_{PS} = \sum_{m=1}^{12}\left(\frac{P_m}{P} - \frac{1}{12}\right)\Delta\delta^{18}O_m \quad (7)$$

$\Delta\delta^{18}O_{ann}$ is the (arithmetic) mean annual of the change of isotopic composition and is completely independent of seasonal cycle. The residual seasonality term $\Delta\delta^{18}O_{PS}$ reflects the change of isotopic composition weighted by the seasonal cycle of precipitation climatology. Since $\sum_{m=1}^{12}\left(\frac{P_m}{P} - \frac{1}{12}\right) = 0$, this term can be rewritten as

$$\Delta\delta^{18}O_{PS} = \sum_{m=1}^{12}\left(\frac{P_m}{P} - \frac{1}{12}\right)(\Delta\delta^{18}O_m - \Delta\delta^{18}O_{ann}) \quad (8)$$

The sign of this term is determined by the dominant season of $\Delta\delta^{18}O_m$ response. In the case of HS1 or YD, the response of isotopic composition is dominated by the depletion in winter $\Delta\delta^{18}O_m - \Delta\delta^{18}O_{ann} < 0$, when the snowfall is also below the annual mean, i.e., $\frac{P_m}{P} - \frac{1}{12} < 0$. This leads to an enrichment $\Delta\delta^{18}O_{PS} > 0$ similar to the effect induced by the response of the precipitation seasonality $\Delta P_s > 0$. However, as the product of two relatively smaller deviations, $\Delta\delta^{18}O_{PS}$ is usually small, relative to either $\Delta\delta^{18}O_{ann}$ or ΔP_s over Greenland (Fig. 2A), and, more generally, the Arctic. Thus, $\Delta\delta^{18}O_s$ is dominated by the change of the annual composition

$$\Delta\delta^{18}O_s \approx \Delta\delta^{18}O_{ann} \quad (9)$$

Last, our decomposition is calculated as follows. Assuming two states, 1 and 2, the difference between the two states is decomposed as

$$\begin{aligned}\Delta\delta^{18}O &= (\delta^{18}O)_1 - (\delta^{18}O)_2 = \sum_{i=m}^{12}\left(\frac{P_m}{P}\right)_1(\delta^{18}O_m)_1 - \sum_{m=1}^{12}\left(\frac{P_m}{P}\right)_2(\delta^{18}O_m)_2\\ &\equiv \sum_{i=m}^{12}\left(\frac{P_m}{P}\right)_2\Delta(\delta^{18}O_m) + \sum_{m=1}^{12}\Delta\left(\frac{P_m}{P}\right)(\delta^{18}O_m)_1\\ &\equiv \sum_{m=1}^{12}\left(\frac{P_m}{P}\right)_1\Delta(\delta^{18}O_m) + \sum_{m=1}^{12}\Delta\left(\frac{P_m}{P}\right)(\delta^{18}O_m)_2 \quad (10)\\ &\equiv \sum_{m=1}^{12}\left[\frac{\left(\frac{P_m}{P}\right)_1 + \left(\frac{P_m}{P}\right)_2}{2}\right]\Delta(\delta^{18}O_m) + \sum_{m=1}^{12}\Delta\left(\frac{P_m}{P}\right)\left[\frac{(\delta^{18}O_m)_1 + (\delta^{18}O_m)_2}{2}\right]\end{aligned}$$

Here, we adopt the form

$$\Delta P_s = \sum_{m=1}^{12}\left[\frac{\left(\frac{P_m}{P}\right)_1 + \left(\frac{P_m}{P}\right)_2}{2}\right]\Delta(\delta^{18}O_m) \quad (11)$$

$$\Delta\delta^{18}O_s = \sum_{m=1}^{12}\Delta\left(\frac{P_m}{P}\right)\left[\frac{(\delta^{18}O_m)_1 + (\delta^{18}O_m)_2}{2}\right] \quad (12)$$

with state 1 as that during the deglaciation and state 2 as the LGM.

Given that

$$\begin{aligned}\Delta\delta^{18}O &= \sum_{m=1}^{12}\left(\frac{P_m}{P}\right)_2\Delta(\delta^{18}O_m) + \sum_{m=1}^{12}\Delta\left(\frac{P_m}{P}\right)(\delta^{18}O_m)_2 + \sum_{m=1}^{12}\Delta\left(\frac{P_m}{P}\right)\Delta(\delta^{18}O_m)\\ &\approx \sum_{m=1}^{12}\left(\frac{P_m}{P}\right)_2\Delta(\delta^{18}O_m) + \sum_{m=1}^{12}\Delta\left(\frac{P_m}{P}\right)(\delta^{18}O_m)_2\end{aligned} \quad (13)$$

Our decomposition (Eq. 10) is an approximate decomposition of perturbations on the LGM state.

Comparison of two methods of "filtering" the effect of precipitation seasonality

We have attempted to filter the effect of precipitation seasonality by removing the seasonality terms of ΔP_s and $\Delta\delta^{18}O_{PS}$ and then considering the sensitivity of $\Delta\delta^{18}O_{ann}$ to ΔT. In comparison, some previous works have attempted to filter the effect of precipitation seasonality by considering the sensitivity of ice core $\Delta\delta^{18}O$ to the temperature weighted by precipitation T_p as $\Delta\delta^{18}O/\Delta T_p$ (*31*, *33*). Our analysis of the deglaciation simulation shows that these two methods are qualitatively similar. However, quantitatively, our method is more favorable. Our calculation during the deglaciation shows that $\Delta\delta^{18}O/\Delta T_p$ tends to be larger than $\Delta\delta^{18}O/\Delta T$ (not shown), as in previous work (*31*, *33*), implying a suppression from $\Delta\delta^{18}O/\Delta T_p$ to $\Delta\delta^{18}O/\Delta T$. This suppression is qualitatively consistent with the suppression from $\Delta\delta^{18}O_{ann}/\Delta T$ to $\Delta\delta^{18}O/\Delta T$ in our decomposition method (fig. S3, A, C, and E). However, the magnitude of suppression from $\Delta\delta^{18}O/\Delta T_p$ is substantially smaller than from $\Delta\delta^{18}O_{ann}/\Delta T$ (not shown). Furthermore, the suppression relation of $\Delta\delta^{18}O/\Delta T_p$ is much less robust than $\Delta\delta^{18}O_{ann}/\Delta T$: Over Greenland, the correlation is ~0.5 between $\Delta\delta^{18}O$ and ΔT_p compared with ~0.9 between $\Delta\delta^{18}O_{ann}$ and ΔT. The reason is that T_p overweights the summer precipitation effect into temperature, and therefore, $\Delta\delta^{18}O/\Delta T_p$ tends to be dominated by the summer slope $\Delta\delta^{18}O_{sum}/\Delta T_{sum}$. In contrast, deglacial annual temperature variability ΔT is dominated by winter variability, and therefore, our $\Delta\delta^{18}O_{ann}/\Delta T$ is similar to the winter slope $\Delta\delta^{18}O_{win}/\Delta T_{win}$ and, therefore, is more robust.

Tagging experiments at LGM, H1, BA, and YD

Four water tagging experiments are performed at LGM (20 ka; ExpLGM), H1 (15.5 ka; ExpHS1), BA (13.2 ka; ExpBA), and YD (12.2 ka; ExpYD) in the atmospheric component model of iCESM1.3 (iCAM5.3) to examine the response of moisture source and $\delta^{18}O$. Each experiment is integrated for 40 years with the past 20 years' data analyzed. For each experiment, the model is forced by the climatology of monthly sea ice distribution, SST, and sea surface $\delta^{18}O$ and δD extracted from the iTRACE experiment, as well as the continental ice sheet, orbital parameters, and GHG concentration, the same as in iTRACE. We tagged 25 regions over the globe, including 13 regions in the ocean and 12 over the lands. For the purpose here, we regrouped the 25 regions into four domains, representing the Atlantic Ocean, Pacific Ocean, land in the mid-latitude [including the entire North America, Greenland, Europe (35° to 90°N, 10°S to 60°E), and North Asia (45° to 90°N, 60° to 180°E)], and the rest of globe.

The tagging experiments track the moisture and oxygen isotopes from each source region during its life cycle from evaporation (source) to condensation (sink) such that the precipitation at a grid point of a calendar month m is the sum of precipitation contributed by all the four regions (j = 1,2,3,4)

$$P_m = \Sigma_{j=1}^{4} p_{m,j} \tag{14}$$

and the $\delta^{18}O$ at month m is

$$\delta^{18}O_{\mathrm{m}} = \Sigma_{j=1}^{4} \delta^{18}O_{m,j} \frac{p_{m,j}}{P_m} \tag{15}$$

where the $p_{m,j}$ and $\delta^{18}O_{m,j}$ denote the precipitation and the oxygen isotope composition in the precipitation from source j at month m, respectively.

Sea ice sensitivity experiment

To separate the impacts of sea ice coverage and SST in forcing the climate-isotope response, we performed an extra sensitivity tagging experiment that is the same as ExpBA, except that the sea ice is replaced by that of YD, denoting $\mathrm{ExpBA}_{\mathrm{YD\text{-}seaice}}$. Hence, the response between YD and BA can be decomposed into two parts

$$\begin{aligned}\mathrm{ExpYD-ExpBA} = {} & (\mathrm{ExpBA}_{\mathrm{YD-seaice}} - \mathrm{ExpBA}) + \\ & (\mathrm{ExpYD} - \mathrm{ExpBA}_{\mathrm{YD-seaice}})\end{aligned} \tag{16}$$

On the right-hand side, the first term represents the impact of sea ice forcing, as the setting of $\mathrm{ExpBA}_{\mathrm{YD\text{-}seaice}}$ is identical to that in BA except for the sea ice cover (fig. S8, A to E). The second term represents the role of other forcings, including SST, ice sheet, orbital forcing, ocean surface $\delta^{18}O$ and δD, etc. (fig. S8, F to J). Since $\mathrm{ExpBA}_{\mathrm{YD\text{-}seaice}}$ and ExpYD are performed at 13.2 and 12.2 ka, respectively, the difference of other forcings are minimal except for SST because of the change of AMOC, and the difference in ocean surface $\delta^{18}O$ and δD is also negligible. The second term, therefore, mainly reflects the role of SST. Consistent with the sea ice impact discussed, the sea ice expansion alone leads to a cooling, precipitation reduction, and depletion in oxygen isotopic composition $\delta^{18}O_{\mathrm{ann}}$ over Greenland, which is suppressed in the precipitation $\delta^{18}O$ (fig. S8, A to E). The SST cooling alone also forces a similar response but with a smaller magnitude.

SUPPLEMENTARY MATERIALS

Supplementary material for this article is available at http://advances.sciencemag.org/cgi/content/full/7/25/eabh1007/DC1

REFERENCES AND NOTES

1. J. Lynch-Stieglitz, The Atlantic meridional overturning circulation and abrupt climate change. *Ann. Rev. Mar. Sci.* **9**, 83–104 (2017).
2. S. Rahmstorf, Ocean circulation and climate during the past 120,000 years. *Nature* **419**, 207–214 (2002).
3. R. B. Alley, P. U. Clark, L. D. Keigwin, R. S. Webb, Making sense of millennial-scale climate change. *Geophys. Monogr. Am. Geophys. Union* **112**, 385–394 (1999).
4. W. Dansgaard, Stable isotopes in precipitation. *Tellus* **16**, 436–468 (1964).
5. E. Böhm, J. Lippold, M. Gutjahr, M. Frank, P. Blaser, B. Antz, J. Fohlmeister, N. Frank, M. B. Andersen, M. Deininger, Strong and deep Atlantic meridional overturning circulation during the last glacial cycle. *Nature* **517**, 73–76 (2015).
6. B. Martrat, J. O. Grimalt, N. J. Shackleton, L. de Abreu, M. A. Hutterli, T. F. Stocker, Four climate cycles of recurring deep and surface water destabilizations on the Iberian margin. *Science* **317**, 502–507 (2007).
7. Y.-J. Wang, H. Cheng, R. L. Edwards, Z. S. An, J. Y. Wu, C.-C. Shen, J. A. Dorale, A high-resolution absolute-dated late Pleistocene monsoon record from Hulu Cave, China. *Science* **294**, 2345–2348 (2001).
8. S. O. Rasmussen, M. Bigler, S. P. Blockley, T. Blunier, S. L. Buchardt, H. B. Clausen, I. Cvijanovic, D. Dahl-Jensen, S. J. Johnsen, H. Fischer, V. Gkinis, M. Gullevic, W. Z. Hoek, J. J. Lowe, J. B. Pedro, T. Popp, I. K. Seierstad, J. P. Steffensen, A. M. Sevensson, P. Vallelonga, B. M. Vinther, M. J. C. Walker, J. J. Wheatley, M. Winstrup, A stratigraphic framework for abrupt climatic changes during the Last Glacial period based on three synchronized Greenland ice-core records: Refining and extending the INTIMATE event stratigraphy. *Quat. Sci. Rev.* **106**, 14–28 (2014).
9. P. U. Clark, J. D. Shakun, P. A. Baker, P. J. Bartlein, S. Brewer, E. J. Brook, A. E. Carlson, H. Cheng, D. S. Kaufman, Z. Lui, T. M. Marchitto, A. C. Mix, C. Morrill, B. L. Otto-Bliesner, K. Pahnke, J. M. Russell, C. Whitlock, J. F. Adkins, J. L. Blois, J. Clark, S. M. Colman, W. B. Curry, B. P. Flower, F. He, T. C. Johnson, J. Lynch-Stieglitz, V. Markgraf, J. F. McManus, J. X. Mitrovica, P. I. Moreno, J. W. Williams, Global climate evolution during the last deglaciation. *Proc. Natl. Acad. Sci. U.S.A.* **109**, E1134–E1142 (2012).
10. J. D. Shakun, P. U. Clark, F. He, S. A. Marcott, A. C. Mix, Z. Liu, B. Otto-Bliesner, A. Schmittner, E. Bard, Global warming preceded by increasing carbon dioxide concentrations during the last deglaciation. *Nature* **484**, 49–54 (2012).
11. J. F. McManus, R. Francois, J. M. Gherardi, L. D. Keigwin, S. Brown-Leger, Collapse and rapid resumption of Atlantic meridional circulation linked to deglacial climate changes. *Nature* **428**, 834–837 (2004).
12. D. A. Hodell, J. A. Nicholl, T. R. R. Bontognali, S. Danino, J. Dorador, J. A. Dowdeswell, J. Einsle, H. Kuhlmann, B. Martrat, M. J. Mleneck-Vautravers, F. J. Rodríguez-Tovar, U. Röhl, Anatomy of Heinrich Layer 1 and its role in the last deglaciation. *Paleoceanography* **32**, 284–303 (2017).
13. P. M. Grootes, M. Stuiver, J. W. C. White, S. Johnsen, J. Jouzel, Comparison of oxygen isotope records from the GISP2 and GRIP Greenland ice cores. *Nature* **366**, 552–554 (1993).
14. G. H. Denton, R. B. Alley, G. C. Comer, W. S. Broecker, The role of seasonality in abrupt climate change. *Quat. Sci. Rev.* **24**, 1159–1182 (2005).
15. E. Bard, F. Rostek, J. L. Turon, S. Gendreau, Hydrological impact of Heinrich events in the subtropical northeast atlantic. *Science* **289**, 1321–1324 (2000).
16. A. Landais, E. Capron, V. Masson-Delmotte, S. Toucanne, R. Rhodes, T. Popp, B. Vinther, B. Minster, F. Prié, Ice core evidence for decoupling between midlatitude atmospheric water cycle and Greenland temperature during the last deglaciation. *Clim. Past* **14**, 1405–1415 (2018).
17. E. Brady, S. Stevenson, D. Bailey, Z. Liu, D. Noone, J. Nusbaumer, B. L. Otto-Bliesner, C. Tabor, R. Tomas, T. Wong, J. Zhang, J. Zhu, The connected isotopic water cycle in the community earth system model version 1. *J. Adv. Model. Earth Syst.* **11**, 2547–2566 (2019).
18. C. He, Z. Liu, B. L. Otto-Bliesner, E. C. Brady, C. Zhu, R. Tomas, P. U. Clark, J. Zhu, A. Jahn, S. Gu, J. Zhang, J. Nusbaumer, D. Noone, H. Cheng, Y. Wang, M. Yan, Y. Bao, Hydroclimate footprint of pan-Asian monsoon water isotope during the last deglaciation. *Sci. Adv.* **7**, eabe2611 (2021).
19. K. M. Cuffey, G. D. Clow, R. B. Alley, M. Stuiver, E. D. Waddington, R. W. Saltus, Large arctic temperature change at the Wisconsin-Holocene glacial transition. *Science* **270**, 455–458 (1995).
20. V. Masson-Delmotte, J. Jouzel, A. Landais, M. Stievenard, S. J. Johnsen, J. W. C. White, M. Werner, A. Sveinbjornsdottir, K. Fuhrer, GRIP deuterium excess reveals rapid and orbital-scale changes in greenland moisture origin. *Science* **309**, 118–121 (2005).
21. C. Buizert, V. Gkinis, J. P. Severinghaus, F. He, B. S. Lecavalier, P. Kindler, M. Leuenberger, A. E. Carlson, B. Vinther, V. Masson-Delmotte, J. W. C. White, Z. Liu, B. Otto-Bliesner,

E. J. Brook, Greenland temperature response to climate forcing during the last deglaciation. *Science* **345**, 1177–1180 (2014).
22. J. A. Badgeley, E. J. Steig, G. J. Hakim, T. J. Fudge, Greenland temperature and precipitation over the last 20 000 years using data assimilation. *Clim. Past* **16**, 1325–1346 (2020).
23. Z. Liu, B. L. Otto-Bliesner, F. He, E. C. Brady, R. Tomas, P. U. Clark, A. E. Carlson, J. Lynch-Stieglitz, W. Curry, E. Brook, D. Erickson, R. Jacob, J. Kutzbach, J. Cheng, Transient simulation of last deglaciation with a new mechanism for bolling-allerod warming. *Science* **325**, 310–314 (2009).
24. B. L. Otto-Bliesner, E. C. Brady, The sensitivity of the climate response to the magnitude and location of freshwater forcing: Last glacial maximum experiments. *Quat. Sci. Rev.* **29**, 56–73 (2010).
25. F. He, J. D. Shakun, P. U. Clark, A. E. Carlson, Z. Liu, B. L. Otto-Bliesner, J. E. Kutzbach, Northern Hemisphere forcing of Southern Hemisphere climate during the last deglaciation. *Nature* **494**, 81–85 (2013).
26. M. Kageyama, U. Merkel, B. Otto-Bliesner, M. Prange, A. Abe-Ouchi, G. Lohmann, R. Ohgaito, D. M. Roche, J. Singarayer, D. Swingedouw, X. Zhang, Climatic impacts of fresh water hosing under Last Glacial Maximum conditions: A multi-model study. *Clim. Past* **9**, 935–953 (2013).
27. P. J. Fawcett, A. M. Ágústsdóttir, R. B. Alley, C. A. Shuman, The Younger Dryas termination and North Atlantic Deep Water formation: Insights from climate model simulations and Greenland ice cores. *Paleoceanography* **12**, 23–38 (1997).
28. K. M. Cuffey, G. D. Clow, Temperature, accumulation, and ice sheet elevation in central Greenland through the last deglacial transition. *J. Geophys. Res. Oceans* **102**, 26383–26396 (1997).
29. G. Krinner, C. Genthon, J. Jouzel, GCM analysis of local influences on ice coreδsignals. *Geophys. Res. Lett.* **24**, 2825–2828 (1997).
30. J. Jouzel, R. B. Alley, K. M. Cuffey, W. Dansgaard, P. Grootes, G. Hoffmann, S. J. Johnsen, R. D. Koster, D. Peel, C. A. Shuman, M. Stievenard, M. Stuiver, J. White, Validity of the temperature reconstruction from water isotopes in ice cores. *J. Geophys. Res. Oceans* **102**, 26471–26487 (1997).
31. M. Werner, U. Mikolajewicz, M. Heimann, G. Hoffmann, Borehole versus isotope temperatures on Greenland: Seasonality does matter. *Geophys. Res. Lett.* **27**, 723–726 (2000).
32. C. Li, D. S. Battisti, D. P. Schrag, E. Tziperman, Abrupt climate shifts in Greenland due to displacements of the sea ice edge. *Geophys. Res. Lett.* **32**, 1–4 (2005).
33. F. S. R. Pausata, M. Löfverström, On the enigmatic similarity in Greenland $\delta^{18}O$ between the Oldest and Younger Dryas. *Geophys. Res. Lett.* **42**, 10,470–10,477 (2015).
34. L. C. Sime, P. O. Hopcroft, R. H. Rhodes, Impact of abrupt sea ice loss on Greenland water isotopes during the last glacial period. *Proc. Natl. Acad. Sci. U.S.A.* **116**, 4099–4104 (2019).
35. J. P. Severinghaus, T. Sowers, E. J. Brook, R. B. Alley, M. L. Bender, Timing of abrupt climate change at the end of the Younger Dryas interval from thermally fractionated gases in polar ice. *Nature* **391**, 141–146 (1998).
36. G. R. Bromley, A. E. Putnam, K. M. Rademaker, T. V. Lowell, J. M. Schaefer, B. Hall, G. Winckler, S. D. Birkel, H. W. Borns, Younger Dryas deglaciation of Scotland driven by warming summers. *Proc. Natl. Acad. Sci. U.S.A.* **111**, 6215–6219 (2014).
37. H. E. Wittmeier, J. M. Schaefer, J. Bakke, S. Rupper, Ø. Paasche, R. Schwartz, R. C. Finkel, Late Glacial mountain glacier culmination in Arctic Norway prior to the Younger Dryas. *Quat. Sci. Rev.* **245**, 106461 (2020).
38. P. Kindler, M. Guillevic, M. Baumgartner, J. Schwander, A. Landais, M. Leuenberger, Temperature reconstruction from 10 to 120 kyr b2k from the NGRIP ice core. *Clim. Past* **10**, 887–902 (2014).
39. Z. Liu, A. E. Carlson, F. He, E. C. Brady, B. L. Otto-Bliesner, B. P. Briegleb, M. Wehrenberg, P. U. Clark, S. Wu, J. Cheng, J. Zhang, D. Noone, J. Zhu, Younger Dryas cooling and the Greenland climate response to CO_2. *Proc. Natl. Acad. Sci. U.S.A.* **109**, 11101–11104 (2012).
40. J. W. Hurrell, M. M. Holland, P. R. Gent, S. Ghan, J. E. Kay, P. J. Kushner, J. F. Lamarque, W. G. Large, D. Lawrence, K. Lindsay, W. H. Lipscomb, M. C. Long, N. Mahowald, D. R. Marsh, R. B. Neale, P. Rasch, S. Vavrus, M. Vertenstein, D. Bader, W. D. Collins, J. J. Hack, J. Kiehl, S. Marshall, The community earth system model: A framework for collaborative research. *Bull. Am. Meteorol. Soc.* **94**, 1339–1360 (2013).
41. A. De Vernal, F. Eynaud, M. Henry, C. Hillaire-Marcel, L. Londeix, S. Mangin, J. Matthießen, F. Marret, T. Radi, A. Rochon, S. Solignac, J.-L. Turon, Reconstruction of sea-surface conditions at middle to high latitudes of the Northern Hemisphere during the Last Glacial Maximum (LGM) based on dinoflagellate cyst assemblages. *Quat. Sci. Rev* **24**, 897–924 (2005).
42. M. Kucera, M. Weinelt, T. Kiefer, U. Pflaumann, A. Hayes, M. Weinelt, M.-T. Chen, A. C. Mix, T. T. Barrows, E. Cortijo, J. Duprat, S. Juggins, C. Wailbroeck, Reconstruction of sea-surface temperatures from assemblages of planktonic foraminifera: Multi-technique approach based on geographically constrained calibration data sets and its application to glacial Atlantic and Pacific Oceans. *Quat. Sci. Rev.* **24**, 951–998 (2005).
43. A. L. Berger, Long-term variations of daily insolation and Quaternary climatic changes. *J. Atmos. Sci.* **35**, 2362–2367 (1978).
44. D. Lüthi, M. Le Floch, B. Bereiter, T. Blunier, J. M. Barnola, U. Siegenthaler, D. Raynaud, J. Jouzel, H. Fischer, K. Kawamura, T. F. Stocker, High-resolution carbon dioxide concentration record 650,000-800,000 years before present. *Nature* **453**, 379–382 (2008).
45. A. Sima, A. Paul, M. Schulz, J. Oerlemans, Modeling the oxygen-isotopic composition of the North American Ice Sheet and its effect on the isotopic composition of the ocean during the last glacial cycle. *Geophys. Res. Lett.* **33**, L15706 (2006).
46. W. R. Peltier, D. F. Argus, R. Drummond, Space geodesy constrains ice age terminal deglaciation: The global ICE-6G_C (VM5a) model. *J. Geophys. Res. Solid Earth* **120**, 450–487 (2015).
47. C. Buizert, B. A. Keisling, J. E. Box, F. He, A. E. Carlson, G. Sinclair, R. M. DeConto, Greenland-wide seasonal temperatures during the last deglaciation. *Geophys. Res. Lett.* **45**, 1905–1914 (2018).
48. D. S. Battisti, Q. Ding, G. H. Roe, Coherent pan-Asian climatic and isotopic response to orbital forcing of tropical insolation. *J. Geophys. Res.* **119**, 11,997–12,020 (2014).
49. I. K. Seierstad, P. M. Abbott, M. Bigler, T. Blunier, A. J. Bourne, E. Brook, S. L. Buchardt, C. Buizert, H. B. Clausen, E. Cook, D. Dahl-Jensen, S. M. Davies, M. Guillevic, S. J. Johnsen, D. S. Pedersen, T. J. Popp, S. O. Rasmussen, J. P. Severinghaus, A. Svensson, B. M. Vinther, Consistently dated records from the Greenland GRIP, GISP2 and NGRIP ice cores for the past 104 ka reveal regional millennial-scale $\delta^{18}O$ gradients with possible Heinrich event imprint. *Quat. Sci. Rev.* **106**, 29–46 (2014).
50. K. K. Andersen, N. Azuma, J.-M. Barnola, M. Bigler, P. Biscaye, N. Caillon, J. Chappellaz, H. B. Clausen, D. Dahl-Jensen, H. Fischer, J. Flückiger, D. Fritzsche, Y. Fujii, K. Goto-Azuma, K. Grønvold, N. S. Gundestrup, M. Hansson, C. Huber, C. S. Hvidberg, S. J. Johnsen, U. Jonsell, J. Jouzel, S. Kipfstuhl, A. Landais, M. Leuenberger, R. Lorrain, V. Masson-Delmotte, H. Miller, H. Motoyama, H. Narita, T. Popp, S. O. Rasmussen, D. Raynaud, R. Rothlisberger, U. Ruth, D. Samyn, J. Schwander, H. Shoji, M.-L. Siggard-Andersen, J. P. Steffensen, T. Stocker, A. E. Sveinbjörnsdóttir, A. Svensson, M. Takata, J.-L. Tison, T. Thorsteinsson, O. Watanabe, F. Wilhelms, J. W. C. White; North Greenland Ice Core Project Members, High-resolution record of Northern Hemisphere climate extending into the last interglacial period. *Nature* **431**, 147–151 (2004).
51. NEEM Community members, Eemian interglacial reconstructed from a Greenland folded ice core. *Nature* **493**, 489–494 (2013).
52. B. M. Vinther, H. B. Clausen, D. A. Fisher, R. M. Koerner, S. J. Johnsen, K. K. Andersen, D. Dahl-Jensen, S. O. Rasmussen, J. P. Steffensen, A. M. Svensson, Synchronizing ice cores from the Renland and Agassiz ice caps to the Greenland Ice Core Chronology. *J. Geophys. Res.* **113**, (2008).
53. B. M. Vinther, H. B. Clausen, S. J. Johnsen, S. O. Rasmussen, K. K. Andersen, S. L. Buchardt, D. Dahl-Jensen, I. K. Seierstad, M.-L. Siggaard-Andersen, J. P. Steffensen, A. Svensson, J. Olsen, J. Heinemeier, A synchronized dating of three Greenland ice cores throughout the Holocene. *J. Geophys. Res.* **111**, (2006).

Acknowledgments: We thank A. Carlson for discussions. **Funding:** This work is supported by Chinese NSFC 41630527; U.S. NSF 1810682, 1810681, and 1702920; and the Qingdao Pilot National Laboratory for Marine Science and Technology. The CESM project is supported primarily by the NSF. This material is based on work supported by the National Center for Atmospheric Research, which is a major facility sponsored by the NSF under Cooperative Agreement no. 1852977. Computing and data storage resources, including the Cheyenne supercomputer (doi: 10.5065/D6RX99HX), were provided by the Computational and Information Systems Laboratory (CISL) at NCAR. **Author contributions:** Z.L. and C.H. conceived this study and wrote the paper. C.H. performed the analysis. C.H., E.C.B., R.T., and C.Z. performed the experiments. C.B. and J.P.S. contributed to proxy interpretations. All authors discussed the results and contributed to the manuscript. **Competing interests:** The authors declare that they have no competing interests. **Data and materials availability:** All data needed to evaluate the conclusions in the paper are present in the paper and/or the Supplementary Materials. All model data supporting our findings are archived at https://doi.org/10.5281/zenodo.4320072 and https://doi.org/10.5281/zenodo.3930129. Paleoclimate proxy data could be found from NOAA (www.ncdc.noaa.gov/data-access/paleoclimatology-data). The code for the present study is available in XCESM (https://github.com/Yefee/xcesm) and xMCA repository (https://github.com/Yefee/xMCA, MCA analysis). Additional data related to this paper may be requested from the authors.

Submitted 16 February 2021
Accepted 29 April 2021
Published 16 June 2021
10.1126/sciadv.abh1007

Citation: C. He, Z. Liu, B. L. Otto-Bliesner, E. C. Brady, C. Zhu, R. Tomas, C. Buizert, J. P. Severinghaus, Abrupt Heinrich Stadial 1 cooling missing in Greenland oxygen isotopes. *Sci. Adv.* **7**, eabh1007 (2021).

Science Advances

Abrupt Heinrich Stadial 1 cooling missing in Greenland oxygen isotopes

Chengfei He, Zhengyu Liu, Bette L. Otto-Bliesner, Esther C. Brady, Chenyu Zhu, Robert Tomas, Christo Buizert and Jeffrey P. Severinghaus

Sci Adv **7** (25), eabh1007.
DOI: 10.1126/sciadv.abh1007

Science Advances (ISSN 2375-2548) is published by the American Association for the Advancement of Science, 1200 New York Avenue NW, Washington, DC 20005. The title *Science Advances* is a registered trademark of AAAS.